Mitochondrial fission protein 1 up-regulation ameliorates senescence-related endothelial dysfunction of human endothelial progenitor cells

Hsueh-Hsiao Wang[1,*] , Yih-Jer Wu[1,2], Ya-Ming Tseng[1], Cheng-Huang Su[1,2], Chin-Ling Hsieh[2], Hung-I Yeh[1,2]

[1] *Department of Medicine, Mackay Medical College, New Taipei City, Taiwan*
[2] *Departments of Internal Medicine and Medical Research, MacKay Memorial Hospital, Taipei, Taiwan*

Corresponding Author
Hsueh-Hsiao Wang
Department of Medicine, Mackay Medical College, No. 46, Sec. 3, Zhongzheng Rd, Sanzhi District, New Taipei City 252, Taiwan.
Telephone: + 886 2 2636 0303 ext 1224.
Fax: + 886 2 2636 1295.
E-mail: okul.wang@gmail.com; school@mmc.edu.tw
ORCID iD: https://orcid.org/0000-0002-3100-0121

Supplementary Data

1. Supplementary Materials and Methods

1.1 Real-time PCR

After treatment, siRNA and virus mixture was replaced with fresh culture medium for recovery. At indicated time points, total RNA from EPCs were extracted using RNeasy Plus mini kit (Qiagen, Hilden, Germany). Two μg of RNA was applied to the reaction of reverse transcription using iScript cDNA Synthesis kit (BioRad), and 0.5 μl of the cDNA products was used for quantitative PCR amplification with specific primers for Fis1, optic atrophy 1 (OPA1), mitofusin 1 (MFN1), mitochondrial protein 18 kDa (MTP18), sirtuin 1 (SirT1), and β-actin. To conduct real-time PCR, iQ™ SYBR Green Supermix reagent and iQ™ Single Color Real-Time PCR Detector System (all from Bio-Rad) were used. Relative mRNA levels were normalized with the corresponding levels of β-actin. At least three independent experiments were performed for analysis.

1.2 Western blot

At indicated time points, EPCs were washed and lysed with SB-20 buffer (0.69 mol/L SDS, 10 mmol/L EDTA, 100 mmol/L Tris-HCl, pH 6.8). Protein concentrations were determined with modified Lowry's method (Bio-Rad DC protein assay kit). Aliquots of cell lysates were loaded into 10 or 12% SDS-polyacrylamide gels, electrophoresed, and transblotted onto PVDF membranes (Millipore). The blots were blocked with 0.1 g/mL bovine serum albumin (BSA) for 1 hour and detected with primary antibodies (listed in supplementary Table S2). The blots were further incubated with alkaline phosphatase-conjugated secondary antibodies for 1 hour at room temperature. Immunoreactivity was visualized using VisioGlo (Amresco, Solon, Ohio, USA) according to the manufacturer's instruction. The radiographs were subject to TotalLab software (Nonlinear Dynamics, Newcastle upon Tyne, UK). To normalize the expression level, blots were stripped with stripping buffer (69 mmol/L SDS, 100 mmol/L 2-mercaptoethanol, 93.75 mmol/L Tris-HCl, pH 6.8) at 56°C, and incubated with anti-β-actin antibody (1:5000; Abcam) as internal control.

1.3 Cell proliferation analysis

Cell doubling time was measured using the CCK-8 assay (Sigma Aldrich) and cell number counting. Cells with different passage number were seeded onto 24-well plates coated with 1% gelatin. After the seeding, medium were replaced with CCK-8 containing medium at the time points of 2, 26, 50, 74 hours followed by 2 hours incubation at 37°C. The culture media were aspirated and subject to absorbance measurement at 450 nm with 630 nm reference. In addition, the cells were trypsinized,

collected, and counted using trypan blue. At least 3 independent experiments were conducted for each group of cells.

1.4 ATP and ADP/ATP ratio measurement

ATP level in senescent, Fis1 siRNA-treated, and Fis1-transduced EPCs was measured using ATP bioluminescence assay kit CLS II (Roche). After indicated time points, cells on 6-cm culture dish were collected and lysed with 600 μl assay medium (100 mM Tris, 4 mM EDTA, pH 7.75), according to the experimental protocols. Cell suspension was incubated for 2 minutes at 100°C and then centrifuged at 1000 × g for 60 seconds followed by ice-cold incubation. 50 μl supernatant was transfered into a 96-well plate and 50 μl luciferase reagent was added by automated injection followed by chemiluminescence measurement and integrated signal for 1 to 10 s. For ADP/ATP ratio measurement, ADP/ATP ratio assay kit was used (Abcam).100 μl ATP reagent was transfered into a 96-well plate followed by chemiluminescence measurement which examined background signal (RLU_A) and 50 μl supernatant was added to acquired ATP level (RLU_B). After 10 minutes incubation, the background luminescence was measured (RLU_C) and 10 μl ADP converting reagent was added immediately followed by luminescence measurement (RLU_D). Subtract RLU_{BC} from RLU_D indicated the level of ADP.

1.5 Measurement of mitochondrial DNA and telomere length

The total DNA, including nuclear DNA and mitochondrial DNA were purified with a PCR purification kit (High Pure PCR template preparation kit, Roche). Twenty ng of total DNA was applied to the quantitative PCR amplification with primers specific for nDNA and mtDNA. The primers were designed to target nDNA (myogenin promoter and RB1) or mtDNA (mtCOX1 and mt8294-8436) [1,2]. Mitochondria content per genome was then calculated as the ratio of the molecules measured with the mtDNA primers and the genomic DNA primers for each sample. Telomere length was measured in triplicate using a quantitative polymerase chain reaction technique [3]. The technique compares signals from the telomere repeat copy number (T; primers Tel1and Tel2) to a single-copy gene 36B4 copy number (S; primers 36B4u and 36B4d) and a relative T/S ratio was calculated. To normalize for interplate variations, standard DNA (derived from HAEC) was located on each plate. All primers were listed in Table S4. At least three independent experiments were performed for analysis

1.6 Bioenergetic profile/ Basal, O_2 leakage, O_2 burst, Non-ATP O_2 consumption

The bioenergetic profile of EPCs were evaluated using extracellular flux assay kit and XF24 bioanalyzer (both from Seahorse Bioscience, MA, USA). Briefly, cells were trypsinized, collected,

counted using trypan blue, and seeded onto a 24-well assay plate coated with 1% gelatin before the day of analysis. Two hours post seeding, medium was added to the final volume of 500 µl. Twelve hours post inoculation, 500 µl glucose-free conditioned medium was added followed by 2 hours incubation at 37℃. The culture medium was then replaced with 500 µl assay medium (Seahorse Bioscience) and subject to bioenergetic analysis. The stages of O_2 leakage, O_2 burst, and non-ATP O_2 consumption were achieved using oligomycin (2 µmole/L), carbonyl cyanide m-chlorophenyl hydrazone (CCCP, 25 µmole/L), and antimycin A (5 µmole/L, all from Sigma Aldrich), respectively.

1.7 Flow cytometry analysis

The fluorescent dyes used in this study were added to cell medium at indicated concentrations (listed in the supplementary Table S3). After 30 minutes incubation, cells were washed with HBSS, resuspended by trypsinization and analysed immediately using a FACScan flow cytometer (BD FACSCalibur™, BD Bioscience, CA, USA).

1.8 Elucidate mitochondria membrane potential by flow cytometry analysis

The mitochondria membrane potential in cells were evaluated using JC-10 dye (AAT BioQuest, CA, USA) to reflect the mitochondria membrane potential in the cells. Cells were washed with HBSS, resuspended by trypsinization and counted. Each tube had $2x10^5$ cells incubated with JC-10 dye at a final concentration of 10 µmol/L for 30 minutes. After incubation, cells were analyzed immediately using a FACScan flow cytometer (Gallios™, Beckman Coulter, CA, USA).

1.9 Electron microscopy

For thin-section electron microscopy, cultured cells were fixed in 2.5% glutaraldehyde in 0.1 mol/L phosphate buffer (pH 7.2) for 1 hour. The specimens were then rinsed in PBS, postfixed in phosphate-buffered 1% OsO4, dehydrated in ethanol, and embedded in Spurrs resin by standard procedures. Thin sections were stained with uranyl acetate and lead citrate and examined with a transmission electron microscope (JEM-1200EXII, JEOL, MA, USA).

Supplementary Tables

Table S1. siRNA sequence used in this study

siRNA	Sequence (5'to 3')	Accession number
Fis1 siRNA1	TTACGGATGTCATCATTGTACTTGC	NM_016068.2
Fis1 siRNA2	CGCGGACGTACTTTAAGGCCTTCTC	NM_016068.2
Nonsense	AATTCTCCGAACGTGTCACGT	

Table S2. Primary antibodies used in this study[4-19]

Antibody	Brand	Dilution	Antibody	Brand	Dilution
Catalase[4]	Epitomics	1:5000	pDrp-1 s616[19]	Cell signaling	1:500
			pDrp-1 s637[19]	Cell signaling	1:500
GPx[5]	Cell signaling	1:1000	Drp-1[14]	Cell signaling	1:1000
			MFF [18]	Cell signaling	1:500
MnSOD[6]	Upstate	1:1000	VDAC[15]	Abcam	1:1000
Cx43[7]	BD Transduction Labs	1:250	OPA-1[16]	BD Transduction Labs	1:1000
Non-p-Cx43[8]	Zymed	1:250	Fis1 (IF)[13]	Genetex	1:500
p16[9]	BD Pharmingen	1:1000	Fis1 (WB)	Sigma	1:250
p21[10]	BD Pharmingen	1:1000	MFN1[17]	Abcam	1:1000
SirT1[11]	Sigma	1:1000	MFN2[17]	Abcam	1:1000
Ki67[12]	Abcam	1:50	Actin[7]	Abcam	1:5000
PCNA[7]	Dako	1:200	CD31, CD34, and CD45[20]	BD Pharmingen	2×10^5 cells/ 5 μL
PGC1-α[13]	Novus	1:1000			

IF, immunofluorescence; WB, western blot.

Table S3. Fluorescence indicators used in this study

Indicator	Abbreviation	Brand	Concentration
5-(and-6)-chloromethyl-2',7'-dichlorodihydrofluorescein diacetate, acetyl ester	DCFDA	Invitrogen CA, USA	10 μmol/L
Dihydroethidium	DHE	Invitrogen CA, USA	5 μmol/L
MitoTracker® Red CMXRos	MTR	Invitrogen CA, USA	25 nmol/L for imaging 200 nmol/L for Flow cytometry
Nonyl Acridine Orange	NAO	Invitrogen CA, USA	100 nmol/L
Fluo-8®AM	Fluo-8	AAT BioQuest, CA, USA	1 μmol/L

Table S4. Real-time PCR primers used in this study

Name	Specificity	Sequence
Tel1	nDNA	GGTTTTTGAGGGTGAGGGTGAGGGTGAGGGTGAGGGT
Tel2	nDNA	TCCCGACTATCCCTATCCCTATCCCTATCCCTATCCCTA
36B4u	nDNA	CAGCAAGTGGGAAGGTGTAATCC
36B4d	nDNA	CCCATTCTATCATCAACGGGTACAA
mt8294-F	mtDNA	CCACTGTAAAGCTAACTTAGCATTAACC
mt8436-R	mtDNA	GTGATGAGGAATAGTGTAAGGAGTATGG
RB1-F	nDNA	CCAGAAAATAAATCAGATGGTATGTAACA
RB1-R	nDNA	TGGTTTAGGAGGGTTGCTTCC
mtCOX1-F	mtDNA	CCC CTG CCATAACCCAATACC A
mtCOX1-R	mtDNA	CCA GCA GCTAGG ACT GGG AGA GA
Myogenin-F	nDNA	AGG TGC TGT CAG GAA GCA AGG A
Myogenin-R	nDNA	TAG GGG GAG GAG GGA ACA AGG A
Fis1-F	cDNA	AAGAGCACGCAGTTTGAG
Fis1-R	cDNA	GCCTTCTCGTATTCCTTG
OPA1-F	cDNA	AGAATCCTAATGCCATCATACTG
OPA1-R	cDNA	ATTATCTGCTGAATCCTGCTTG
MFN1-F	cDNA	GAAATGCTCAAAGGGTGCTC
MFN1-R	cDNA	CGTTGCTGGAGTGGTAGG
MTP18-F	cDNA	GTGTGTGCTGCCTCTCTC
MTP18-R	cDNA	ATCCACCGACCTGTCAATG
SirT1-F	cDNA	ATAGGTTAGGTGGTGAATATGC
SirT1-R	cDNA	CTGAAGAATCTGGTGGTGAAG

Supplementary Figures and Figure Captions

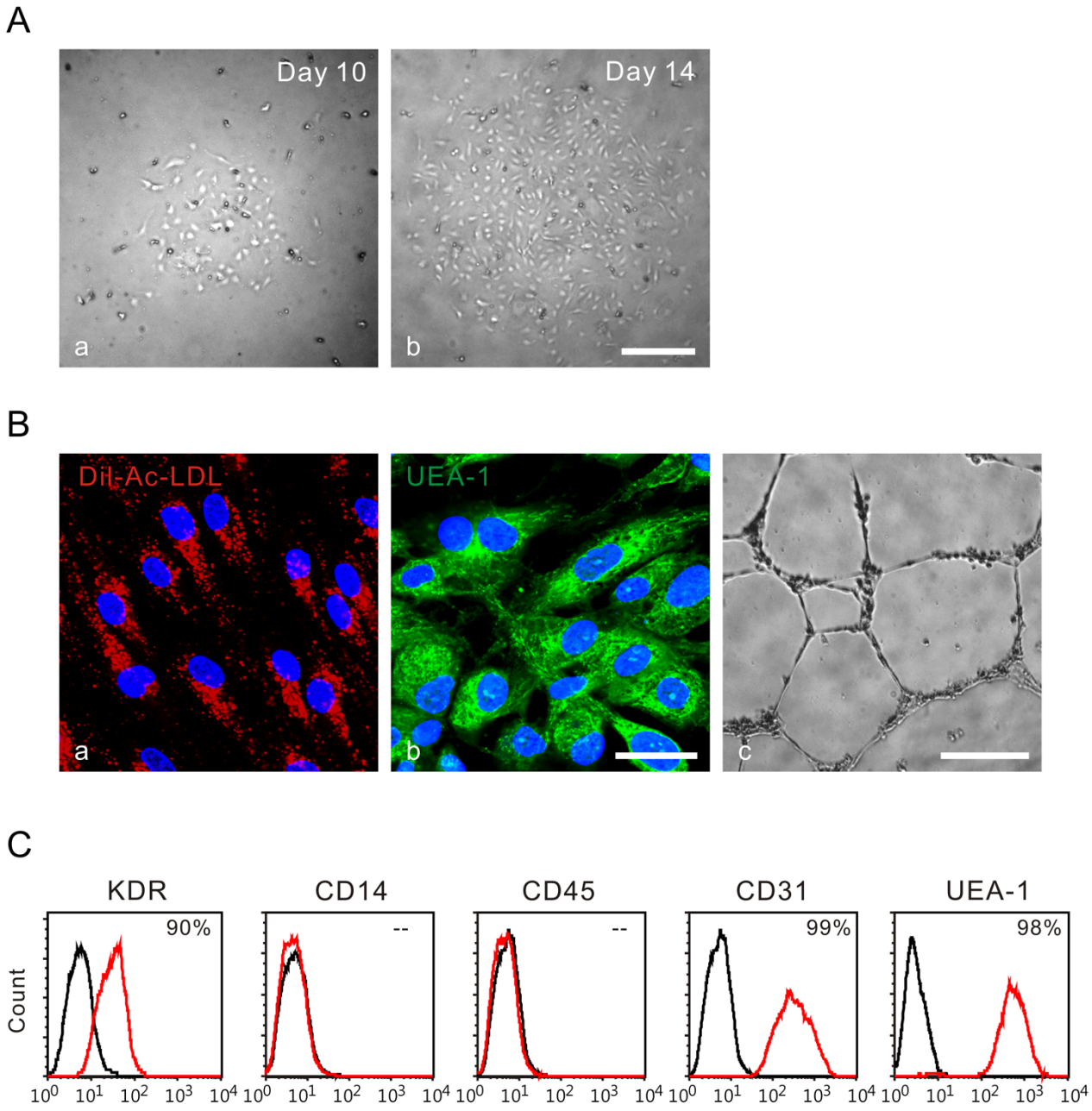

Fig S1. Characterization of human endothelial progenitor cells. After magnetic labeling and separation, isolated CD34-positive cells were maintained with MV2 medium. (A) The phase contrast images of EPC outgrowth were acquired at indicated time points. The endothelial cell properties were examined by Dil-Ac-LDL uptake, UEA-1 binding, and angiogenic potential of tube formation post 20 days culture (B, panels a-c). (C) Flow cytometry analysis showed that the outgrowth cells were positive for KDR, CD31, and UEA-1 but negative for CD14 and CD45. Bars, 300 μm in A and panel c of B; 50 μm in panels a and b of B.

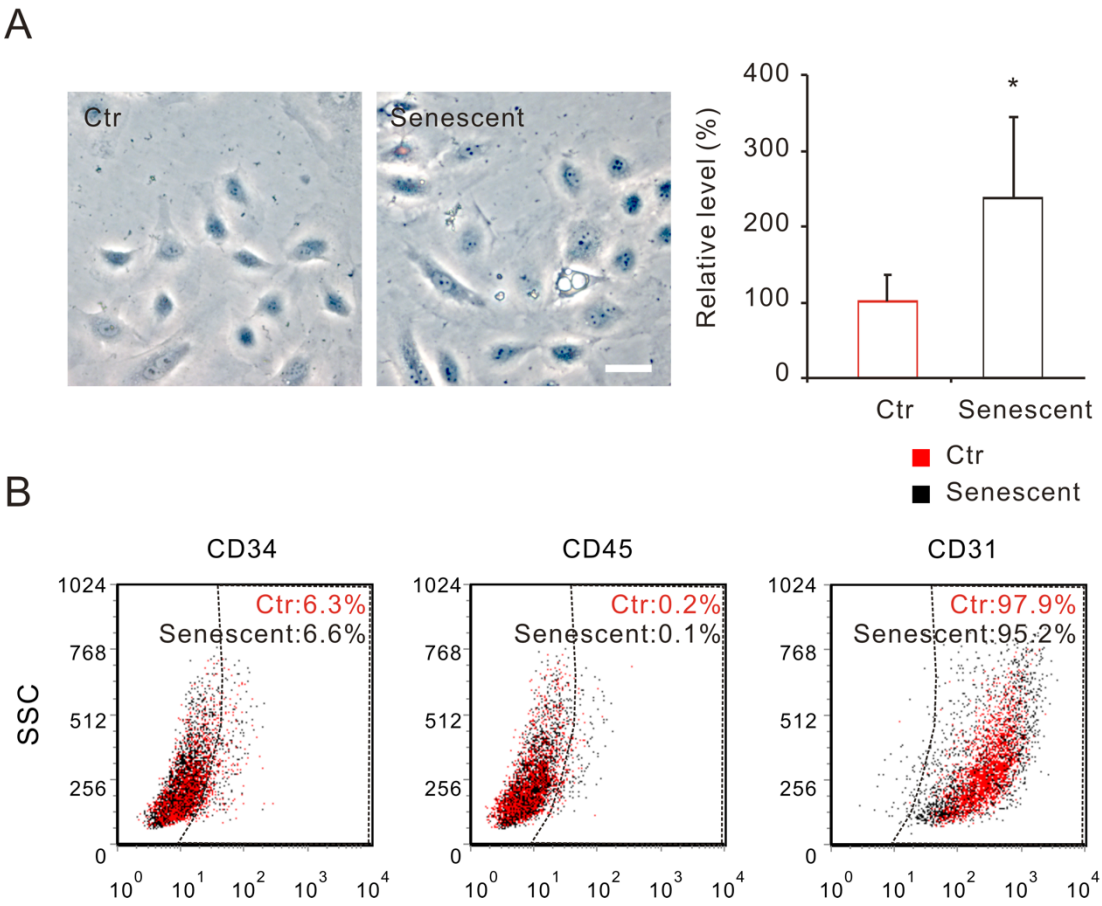

Fig S2. Cellular senescence and surface markers in control (young) and senescent EPCs, as examined using SA-β-Gal staining (A) and flow cytometry (B) followed by analysis. (A) In senescent cells, the β-Gal absorbance increased for more than 130%. (B) Surface markers CD31, CD34, and CD45 exhibited minimal difference between control and senescent groups. The β-Gal absorbance of control group was set as 100%. The result was derived from EPCs of at least three individuals. *, $P<0.05$, compared to the control cells.

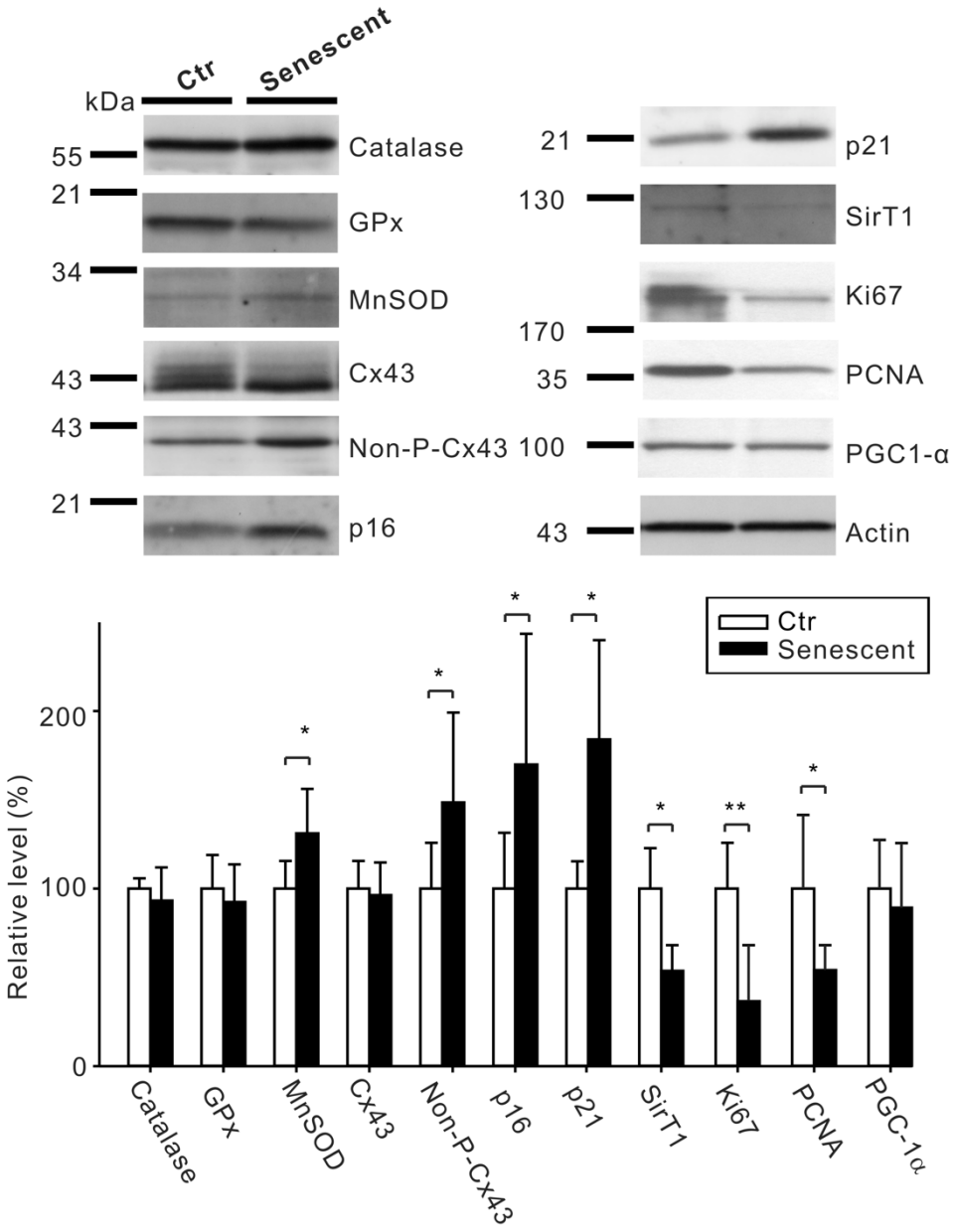

Fig S3. Protein expression profile of senescent human EPCs compared to control (young) cells, as examined using western blotting (A) followed by analysis (B). The protein level of control group was set as 100%. The result was derived from EPCs of at least three individuals. *, $P<0.05$, compared to the control of each molecule.

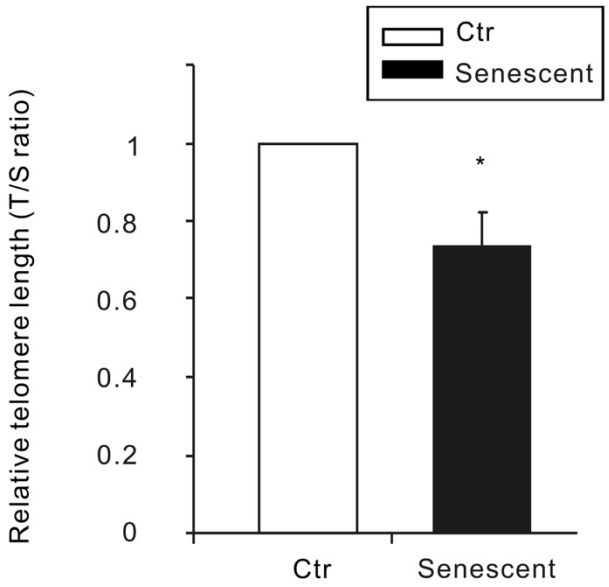

Fig S4. Telomere length in control (young) and senescent EPCs, as examined using real-time PCR. The telomere repeat copy number (T) was normalized to the single-copy gene 36B4 copy number (S). The T/S ratio decreased in the senescent cells. The T/S ratio of control group was set as 1. The result was derived from EPCs of three individuals performed in duplicate. *, P<0.05, compared to the control cells.

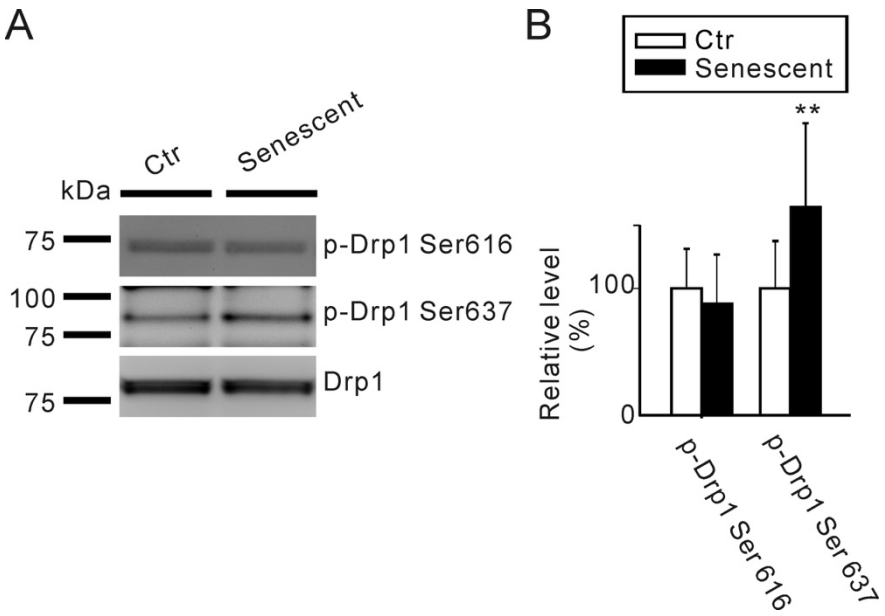

Fig S5. Drp1 phosphorylation profile of senescent human EPCs compared to control (young) cells, as examined using western blotting (A) followed by analysis (B). The phosphorylated protein level of control group was set as 100%. The result was derived from EPCs of at least three individuals. **, P<0.01, compared to the control group of Ser637.

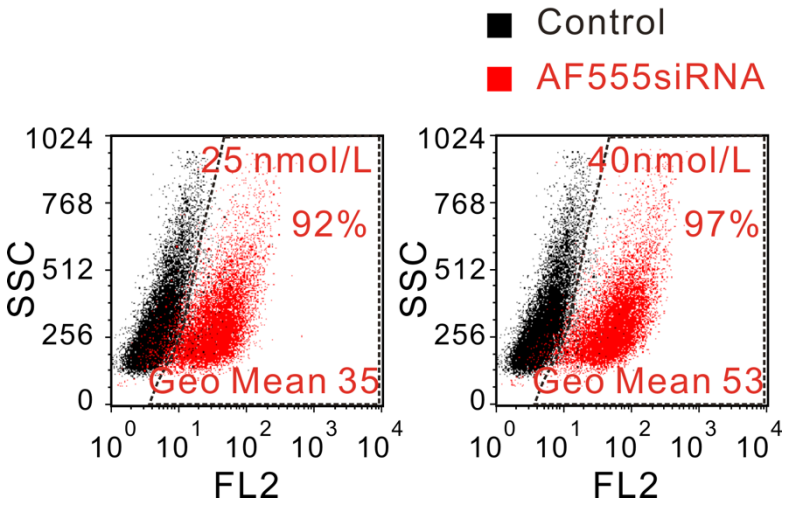

Fig S6. Transfection efficiency of synthetic siRNA in EPCs, as confirmed using flow cytometry. The concentration of alexa fluor 555-labeled synthetic siRNA (in red) was denoted at upper border of each distribution chart. After 5.5 hours of treatment with alexa fluor 555-labeled synthetic siRNA, medium and siRNA-liposome mixture were replaced with fresh medium. Cells were then trypsinized and subject to flow cytometry. The fluorescence distribution profile of cells were shown in black (Control) or red (AF555 siRNA) dots and the fluorescence intensity and percentage of transfected cells, compared to control cells, were calculated. Control, cells with liposome only.

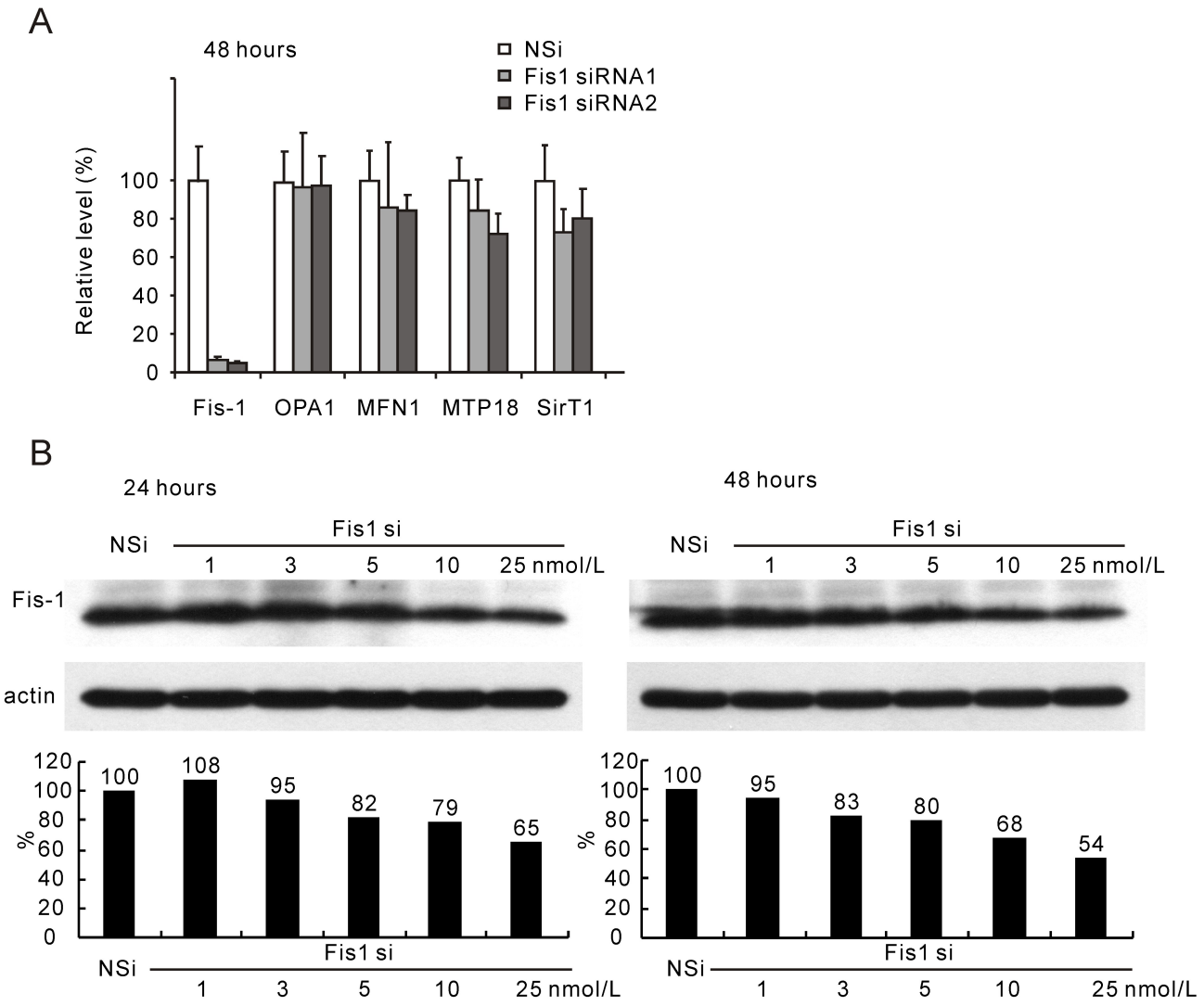
A
48 hours
NSi
Fis1 siRNA1
Fis1 siRNA2
Relative level (%)
0
20
40
60
80
100
Fis-1
OPA1
MFN1
MTP18
SirT1
B
24 hours
48 hours
NSi
Fis1 si
1
3
5
10
25 nmol/L
Fis-1
actin
%
100
108
95
82
79
65
100
95
83
80
68
54
C
NSi/Fis-1
Fis1 siRNA 10 nmol/L
Fis1 siRNA 25 nmol/L
a
b
c
D
72 h
96 h
144 h
240 h
NSi
Fis1si
Fis1
β-actin
Fis1/actin
1.0
0.1
1.0
0.1
1.0
0.1
1.0
0.2

Fig S7. Down-regulation of Fis1 transcript and protein in EPCs treated with synthetic siRNA, as examined using real-time PCR (A), Western blot (B and D), and immunoconfocal microscopy (C). Note that synthetic siRNA specific to Fis1 has minimal effect on the expression level of OPA1, MFN1, MTP18, and SirT1 transcripts. In addition, Fis1 protein is decreased in a dose and time-dependent manner. Fis1-specific siRNA has a lasting effect for over 240 hours (80% decrement). The level of Fis1 in the non-sense group was set as 100%. Bar, 45 μm

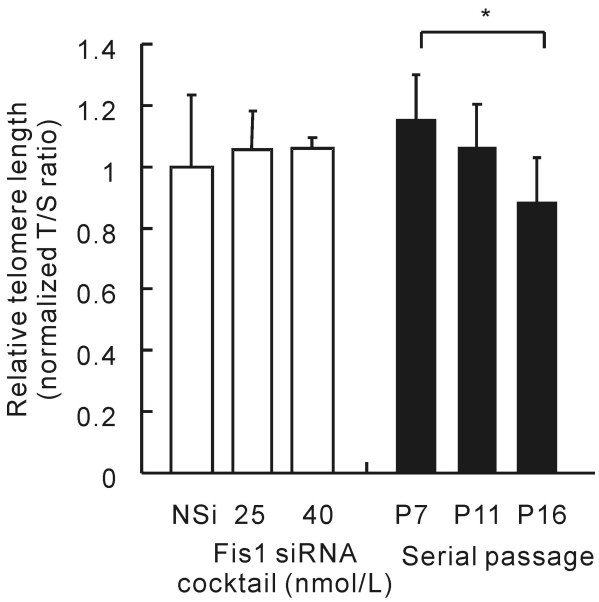

Fig S8. Telomere length in EPCs transfected with Fis1 siRNA, as examined using real-time PCR. The concentrations of Fis1-specific siRNA are labeled and DNA templates derived from EPCs with different passage number 7, 11, and 16 were used as a positive control. The T/S ratio of non-sense (NSi) group was set as 1.

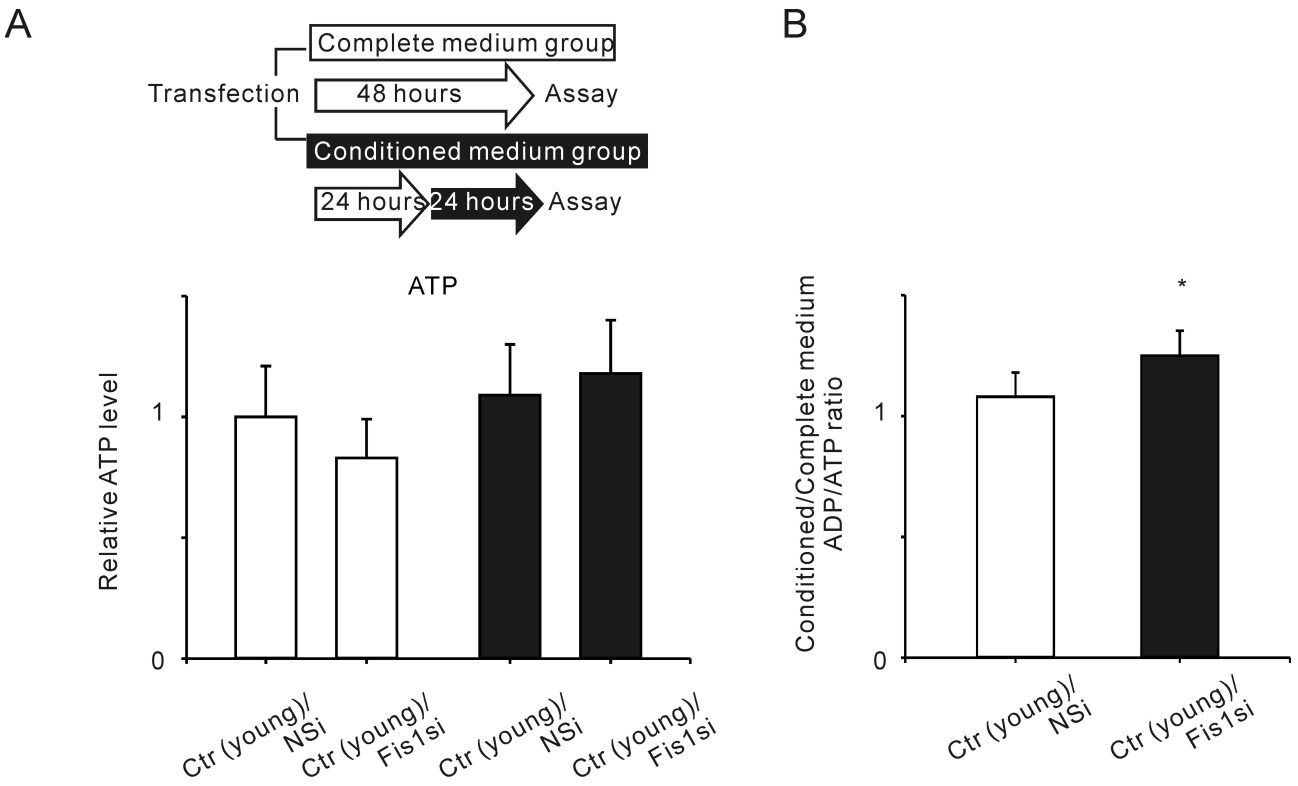

Fig S9. Bioenergetic profile of Fis1-specific siRNA transfected EPCs (N=6) under complete and conditioned medium. ATP level and ADP/ATP ratio are changed in Fis1-specific siRNA transfected cells under conditioned medium. However, the ATP level was minimally changed in the non-sense group (Ctr/NSi, N=6). Under conditioned medium, Fis1 silencing increases the ADP/ATP ratio significantly. See text for details. *, $P<0.05$, compared to control (young) EPCs transfected with non-sense siRNA.

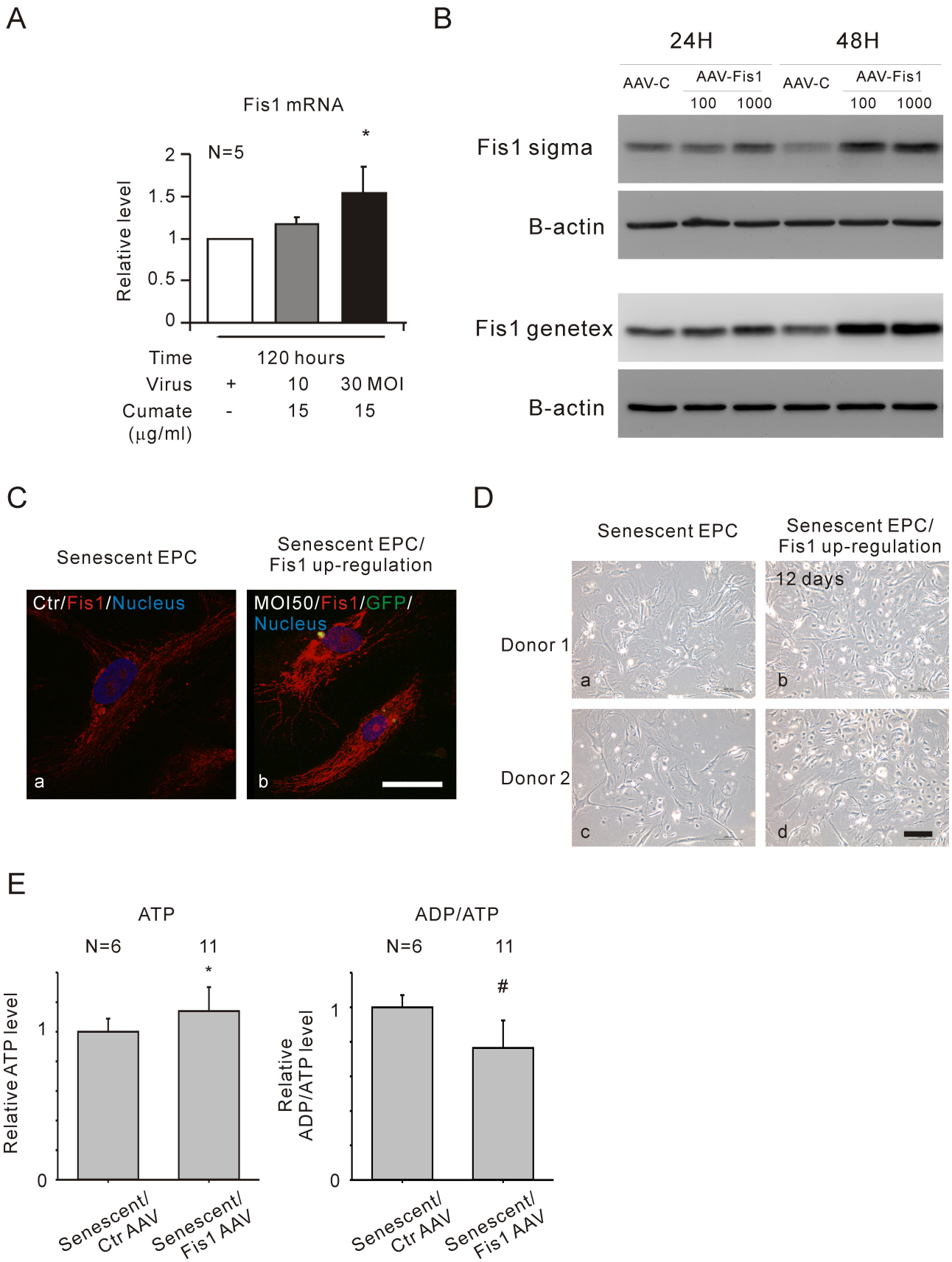

Fig S10. The profile of Fis1 expression, mitochondria structure, cellular appearance, and bioenergetics in Fis1-transfected EPCs, as examined using real-time PCR (A), western blot (B),

confocal microscopy (C), light microscopy after long-term maintenance (D), and ADP/ATP level (E) followed by analysis. Note that Fis1 expression levels are increased in a dose and time-dependent manner. The level of Fis1 in the control group was set as 1. In addition, Fis1 up-regulation restores the senescent EPCs to youthful phenotype, including less elongated mitochondrial structure, higher proliferation activity, cobble stone appearance (confirmed in cells from 2 donors), higher level of ATP, and lower level of ADP/ATP ratio (N=6). *, $P<0.05$; #, $P<0.005$, compared to control bar (senescent cells) of each group. Bars, 40 μm in C; 200 μm in D.

Supplementary reference

1. Andreasson H, Gyllensten U, Allen M (2002) Real-time DNA quantification of nuclear and mitochondrial DNA in forensic analysis. BioTechniques 33 (2):402-404, 407-411. doi:10.2144/02332rr07

2. Rabol R, Svendsen PF, Skovbro M, Boushel R, Haugaard SB, Schjerling P, Schrauwen P, Hesselink MK, Nilas L, Madsbad S, Dela F (2009) Reduced skeletal muscle mitochondrial respiration and improved glucose metabolism in nondiabetic obese women during a very low calorie dietary intervention leading to rapid weight loss. Metabolism: clinical and experimental 58 (8):1145-1152. doi:10.1016/j.metabol.2009.03.014

3. Cawthon RM (2002) Telomere measurement by quantitative PCR. Nucleic acids research 30 (10):e47. doi:10.1093/nar/30.10.e47

4. Lu XY, Liu BC, Wang LH, Yang LL, Bao Q, Zhai YJ, Alli AA, Thai TL, Eaton DC, Wang WZ, Ma HP (2015) Acute ethanol induces apoptosis by stimulating TRPC6 via elevation of superoxide in oxygenated podocytes. Biochimica et biophysica acta 1853 (5):965-974. doi:10.1016/j.bbamcr.2015.01.007

5. Geraghty P, Baumlin N, Salathe MA, Foronjy RF, D'Armiento JM (2016) Glutathione Peroxidase-1 Suppresses the Unfolded Protein Response upon Cigarette Smoke Exposure. Mediators of inflammation 2016:9461289. doi:10.1155/2016/9461289

6. Patki G, Salvi A, Liu H, Atrooz F, Alkadhi I, Kelly M, Salim S (2015) Tempol Treatment Reduces Anxiety-Like Behaviors Induced by Multiple Anxiogenic Drugs in Rats. PLOS ONE 10 (3):e0117498. doi:10.1371/journal.pone.0117498

7. Wang HH, Lin CA, Lee CH, Lin YC, Tseng YM, Hsieh CL, Chen CH, Tsai CH, Hsieh CT, Shen JL, Chan WH, Chang WH, Yeh HI (2011) Fluorescent gold nanoclusters as a biocompatible marker for in vitro and in vivo tracking of endothelial cells. ACS nano 5 (6):4337-4344. doi:10.1021/nn102752a

8. Boulaksil M, Bierhuizen MFA, Engelen MA, Stein M, Kok BJM, van Amersfoorth SCM, Vos MA, van Rijen HVM, de Bakker JMT, van Veen TAB (2016) Spatial Heterogeneity of Cx43 is an Arrhythmogenic Substrate of Polymorphic Ventricular Tachycardias during Compensated Cardiac

Hypertrophy in Rats. Frontiers in cardiovascular medicine 3:5-5. doi:10.3389/fcvm.2016.00005
9. Gizard F, Amant C, Barbier O, Bellosta S, Robillard R, Percevault F, Sevestre H, Krimpenfort P, Corsini A, Rochette J, Glineur C, Fruchart J-C, Torpier G, Staels B (2005) PPAR alpha inhibits vascular smooth muscle cell proliferation underlying intimal hyperplasia by inducing the tumor suppressor p16INK4a. The Journal of clinical investigation 115 (11):3228-3238. doi:10.1172/JCI22756
10. Xu B, Gerin I, Miao H, Vu-Phan D, Johnson CN, Xu R, Chen X-W, Cawthorn WP, MacDougald OA, Koenig RJ (2010) Multiple roles for the non-coding RNA SRA in regulation of adipogenesis and insulin sensitivity. PloS one 5 (12):e14199-e14199. doi:10.1371/journal.pone.0014199
11. Zheng Y, Hu Q, Manaenko A, Zhang Y, Peng Y, Xu L, Tang J, Tang J, Zhang JH (2015) 17beta-Estradiol attenuates hematoma expansion through estrogen receptor alpha/silent information regulator 1/nuclear factor-kappa b pathway in hyperglycemic intracerebral hemorrhage mice. Stroke 46 (2):485-491. doi:10.1161/strokeaha.114.006372
12. Sobecki M, Mrouj K, Camasses A, Parisis N, Nicolas E, Llères D, Gerbe F, Prieto S, Krasinska L, David A, Eguren M, Birling M-C, Urbach S, Hem S, Déjardin J, Malumbres M, Jay P, Dulic V, Lafontaine DL, Feil R, Fisher D (2016) The cell proliferation antigen Ki-67 organises heterochromatin. eLife 5:e13722-e13722. doi:10.7554/eLife.13722
13. Kemter E, Fröhlich T, Arnold GJ, Wolf E, Wanke R (2017) Mitochondrial Dysregulation Secondary to Endoplasmic Reticulum Stress in Autosomal Dominant Tubulointerstitial Kidney Disease - UMOD (ADTKD-UMOD). Scientific reports 7:42970-42970. doi:10.1038/srep42970
14. Zhou Z, Wang Z, Guan Q, Qiu F, Li Y, Liu Z, Zhang H, Dong H, Zhang Z (2016) PEDF Inhibits the Activation of NLRP3 Inflammasome in Hypoxia Cardiomyocytes through PEDF Receptor/Phospholipase A2. International journal of molecular sciences 17 (12):2064. doi:10.3390/ijms17122064
15. Hwang S, Disatnik M-H, Mochly-Rosen D (2015) Impaired GAPDH-induced mitophagy contributes to the pathology of Huntington's disease. EMBO molecular medicine 7 (10):1307-1326. doi:10.15252/emmm.201505256
16. Lee JE, Westrate LM, Wu H, Page C, Voeltz GK (2016) Multiple dynamin family members collaborate to drive mitochondrial division. Nature 540 (7631):139-143. doi:10.1038/nature20555
17. Hsu J-Y, Jhang Y-L, Cheng P-H, Chang Y-F, Mao S-H, Yang H-I, Lin C-W, Chen C-M, Yang S-H (2017) The Truncated C-terminal Fragment of Mutant ATXN3 Disrupts Mitochondria Dynamics in Spinocerebellar Ataxia Type 3 Models. Frontiers in molecular neuroscience 10:196-196. doi:10.3389/fnmol.2017.00196
18. Zhou H, Wang J, Zhu P, Zhu H, Toan S, Hu S, Ren J, Chen Y (2018) NR4A1 aggravates the cardiac microvascular ischemia reperfusion injury through suppressing FUNDC1-mediated mitophagy and promoting Mff-required mitochondrial fission by CK2α. Basic Research in Cardiology 113 (4):23. doi:10.1007/s00395-018-0682-1
19. Janer A, Prudent J, Paupe V, Fahiminiya S, Majewski J, Sgarioto N, Des Rosiers C, Forest A, Lin

Z-Y, Gingras A-C, Mitchell G, McBride HM, Shoubridge EA (2016) SLC25A46 is required for mitochondrial lipid homeostasis and cristae maintenance and is responsible for Leigh syndrome. EMBO molecular medicine 8 (9):1019-1038. doi:10.15252/emmm.201506159
20. Li JY, Su CH, Wu YJ, Tien TY, Hsieh CL, Chen CH, Tseng YM, Shi GY, Wu HL, Tsai CH, Lin FY, Yeh HI (2011) Therapeutic angiogenesis of human early endothelial progenitor cells is enhanced by thrombomodulin. Arteriosclerosis, thrombosis, and vascular biology 31 (11):2518-2525. doi:10.1161/atvbaha.111.235143